A Laboratory Experiment for Demonstrating Post-Coronagraph Wave Front Sensing and Control for Extreme Adaptive Optics

J. Kent Wallace*[a], Randall Bartos[a], Shanti Rao[a], Rocco Samuele[b], Edouard Schmidtlin[a]
[a] Jet Propulsion Laboratory, California Institute of Technology, 4800 Oak Grove Drive, Pasadena, CA, USA 91109;
[b] Northrop Grumman, One Space Park Dr., Redondo Beach, CA USA 90278

ABSTRACT

Direct detection of exo-planets from the ground will become a reality with the advent of a new class of extreme-adaptive optics instruments that will come on-line within the next few years. In particular, the Gemini Observatory will be developing the Gemini Planet Imager (GPI) that will be used to make direct observations of young exo-planets. One major technical challenge in reaching the requisite high contrast at small angles is the sensing and control of residual wave front errors after the starlight suppression system. This paper will discuss the nature of this problem, and our approach to the sensing and control task. We will describe a laboratory experiment whose purpose is to provide a means of validating our sensing techniques and control algorithms. The experimental demonstration of sensing and control will be described. Finally, we will comment on the applicability of this technique to other similar high-contrast instruments

Keywords: Planet detection, coronography, nulling interferometry, wave front sensing.

1. INTRODUCTION

The current state of extra-solar planet detection is both thrilling and taunting: thrilling due to the number of planets discovered[1] and the implication for their abundance in the universe, and taunting because although we have evidence for a great number of them, the techniques are primarily indirect. The planet is inferred from the mutual effect of the planet/sun system upon each other. Direct detection would enable a more rapid determination of planetary companions and, with high-resolution astrometry, a more complete characterization of orbital parameters. A detailed investigation of the spectral content of the planets light would lead to a greater understanding of the planets' atmospheres including their composition, temperatures and gravities. There is much to be gained scientifically by detailed direct observations.

Such observations are beset by several challenges: 1) the very small angular separation of the planet/star and 2) their significant contrast ratio. Challenging as these may be, new classes of coronagraphs and nulling interferometers have been proposed and developed over the last few years to address these concerns. The performance of these high-contrast instruments is now limited by residual systematic error sources. Image plane speckles (due to residual amplitude and phase errors that leak through the coronagraph or nuller) place severe constraints on what would otherwise be detectable.

The small phase and amplitude errors that produce these image plane speckles are neither perfectly static nor perfectly dynamic. If they were entirely static, they could be quantified by observing a calibrator star and simply subtracted from the final image. If they were perfectly dynamic, they would average to a halo that would become more uniform over time. Eventually, the faint planet would imprint itself upon the ever-smoother background. Instead, these image plane speckles tend to change over time scales of typical astronomical observations and so therefore don't lend themselves to either classic calibration or averaging techniques. What has been heretofore lacking is a means of sensing and controlling (removing) these speckles during an observation.

In this paper we give a short description of the nature of these speckles in a classic coronagraph, and describe a method for sensing and controlling these residual errors in a coronagraph. We describe a laboratory experiment that will allow us to simulate and demonstrate this technique. Finally, the application of this technique for the Gemini Planet Imager[2] (GPI) system will be discussed.

*James.K.Wallace@jpl.nasa.gov; phone 1 818 393-7066; fax 1 818 393-3290; www.jpl.nasa.gov

1.1 Principles of calibration wave front sensing in classic coronagraphy

The complex wave front that we expect from a high-contrast adaptive optics system (one with a large number of phase correcting elements and working at very fast sampling and update rates) has only small amplitude and phase errors and can therefore be expanded as follows:

$$E = Ae^{i\varphi} \approx A(1+\varepsilon)(1+i\varphi) \approx A + A(\varepsilon + i\varphi) \tag{1}$$

where terms higher than second order in both the expansion and resulting simplification have been dropped. Transforming this slightly aberrant wave front to a focal plane yields:

$$\Im[E] = \Im[A] + \Im[A(\varepsilon + i\varphi)] = Airy + \Im[A(\varepsilon + i\varphi)] \tag{2}$$

where $\Im[\ ]$ is the fourier transform operator. The effect of a classic coronagraph is to remove the *Airy* component of the above expression[3]. Re-imaging this corongraph-filtered pupil results in an intensity distribution given by the following:

$$I_{pupil} \propto \left|A(\varepsilon + i\varphi)\right|^2 = A^2(\varepsilon^2 + \varphi^2) \tag{3}$$

An optical configuration illustrating such a pupil view coronagraph is shown below.

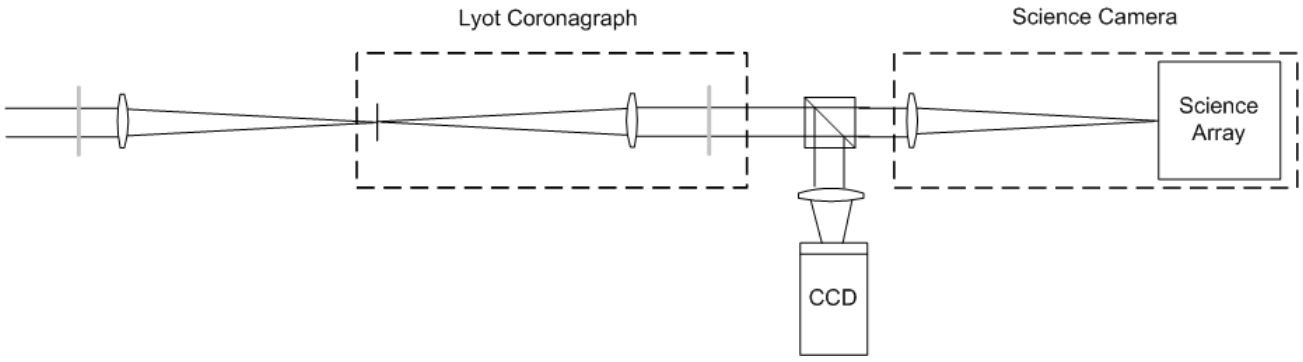

Fig. 1 This illustration shows a cartoon of a simple post-corongraph pupil viewing wave front sensor. As shown above, this camera would see bright pupil speckles anywhere in the pupil where a combination of small amplitude and phase errors remained.

Bright spots in this re-imaged pupil plane could correspond to either residual phase or amplitude effects or a combination of both. Introducing some phase diversity with a deformable mirror element that is conjugate to a bright spot would allow one to determine the contribution due to phase[4] (and thereby minimize it). However, doing so would reduce the observing efficiency of a high-contrast system, as this dithering would reduce the contrast in the final focal plane.

The confusion regarding the type of errors (phase or amplitude) in the above measurement and the magnitude of their contributions can be solved by interfering the post-coronagraph wave front with a reference wave front that is coherent with it[5,6,7]. This reference is conveniently available from the DC term rejected by the coronagraph. An illustration of such an optical system is given below:

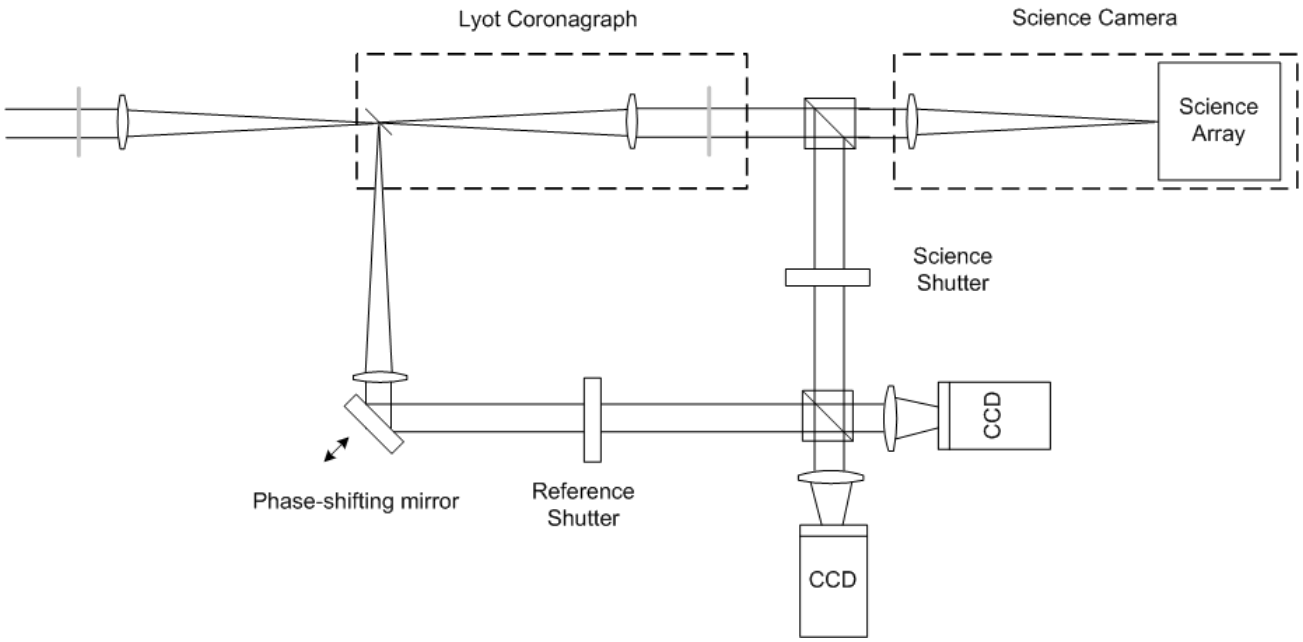

Fig. 2 This image shows how the star-light that is suppressed by the Lyot coronagraph can be used to generate a reference wave front for determining the source of the residual wave front errors. Here we assume that the corongraphic spot is so small that it also acts as a spatial filter. The shutters in the reference and calibration science arms allows us to scale the synchronously demodulated signals appropriately.

If the post-coronagraph wave front is combined with a reference beam that is coherent with it at a re-combination beam splitter we get the following expression:

$$E_{cal} = A(\varepsilon + i\varphi) + Re^{i\theta} \tag{4}$$

The resultant intensity in the image plane is given by the following expression:

$$\begin{aligned} I_{cal} &= \left| A(\varepsilon + i\varphi) + Re^{i\theta} \right|^2 \\ &= A^2(\varepsilon^2 + \varphi^2)R^2 + 2AR\varepsilon\, Cos(\theta) + 2AR\varphi\, Sin(\theta) \end{aligned} \tag{5}$$

If a phase modulation, θ, is applied to the reference wave front and the resulting phase-shifted interferograms recorded, synchronous de-modulation of these calibration images with a Cosine and Sine generated from the same phase modulation will extract the phase and amplitude terms cleanly. Mathematically:

$$\begin{aligned} \left\langle I_{cal} \cdot Cos(\theta) \right\rangle &= AR\varepsilon \\ \left\langle I_{cal} \cdot Sin(\theta) \right\rangle &= AR\varphi \end{aligned} \tag{6}$$

Shuttering the Reference and Science beams separately allows us to measure *A* and *R*, and thus to finally extract the amplitude and phase terms directly.

1.2 Application to calibration wave front sensing to nulling interferometry

The above calibration scheme also lends itself to a nulling-imaging coronagraph[8]. In this type of coronagraph, the wave front from a single aperture is split at an input beamsplitter, sheared, inverted, and then recombined. The shear is introduced to provide an additional position-dependant phase term such that the nulled light at the center of the field transitions to a constructive peak at the planet position. The leakage in such a coronagraph is proportional to the square of the residual phase and amplitude errors in the overlapped, sheared wave fronts at the point of recombination. A deformable mirror internal to the coronagraph can effect a direct correction for the sheared phase difference.

2. POST-CORONAGRAPH WAVE FRONT SENSING TESTBED

2.1 Description of the system

A schematic of the testbed is shown below in Fig. 3. The coronagraph used was the nulling-imaging coronagraph. It is the most well developed coronagraph by our group, and is the one with which we have the most working knowledge. Its choice does not have any particular bearing on the application of this technique to other coronagraphs.

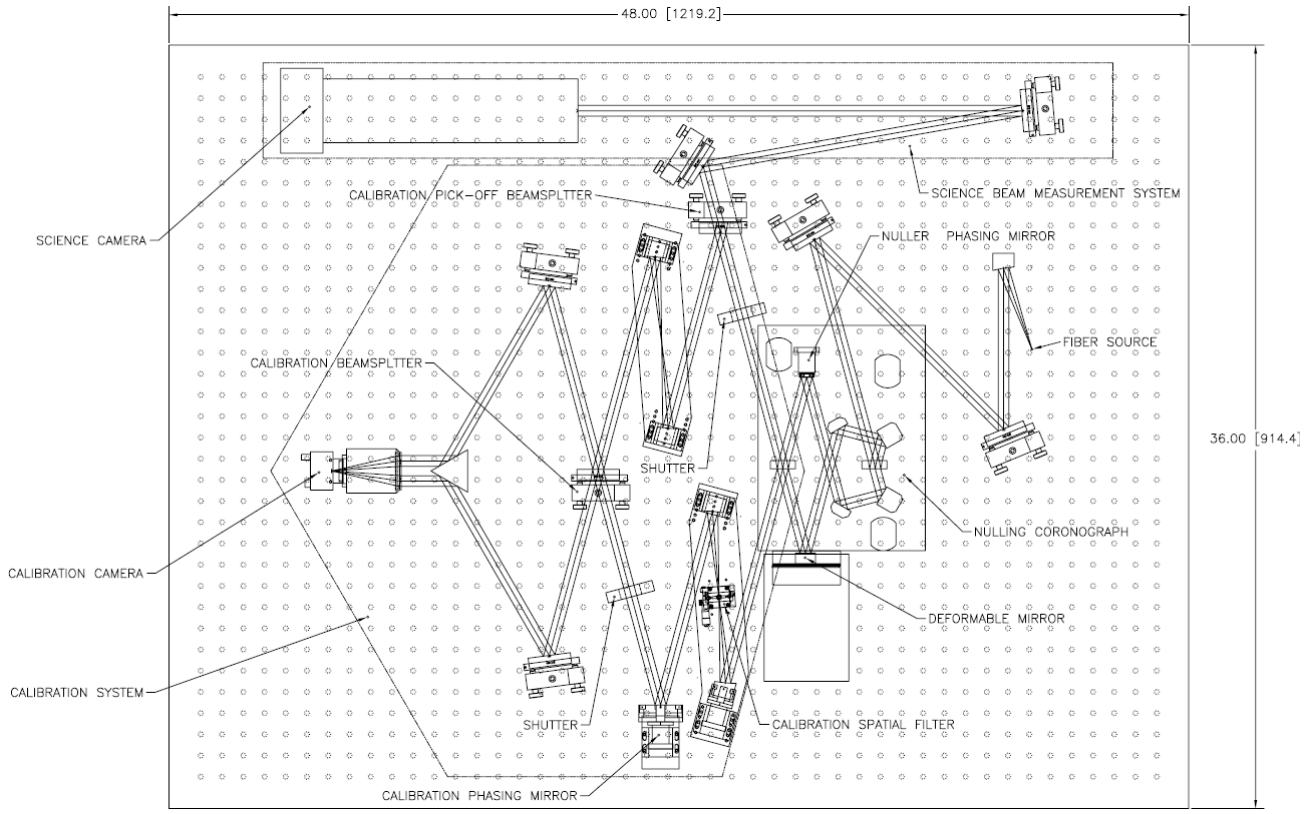

Fig. 3 An image of the detailed opto-mechanical layout of the calibration testbed. This breadboard sets upon sorbothane pucks atop a larger optical table to provide passive vibration isolation.

The optical input into the system is a single-mode optical fiber that serves as an unresolved source. It is collimated with an off-axis parabolic mirror. This arrangement allows us to quickly and easily change the properties of the source without worrying about any potential chromatic side effects. The beam then traverses a pointing/centering mirror pair before striking the first element of nulling coronagraph: a dielectric beam splitter that generates the two arms of the interferometer. The beam that reflects off the beam splitter strikes a set of mirrors that form a right-angle pair, it then strikes the deformable mirror and next the recombination beam splitter. The deformable mirror (DM) is a MEMS device from Boston Micromachines, Inc. Its a 32x32 continuous face-sheet DM with a stroke of about 2 microns. The drive electronics were designed and developed at JPL. The role of the DM is to remove the phase differences between the sheared pupils in the nuller. In the other arm of the interferometer, the light that first passes though the beam splitter hits another right angle pair and then hits the nuller phasing mirror and finally the recombination beam splitter. The nuller phasing mirror is on a PZT stage that has a maximum of 12 microns of stroke with a resolution of 1 nm and a maximum tilt of 1.2 arc minutes. Its purpose is providing fine phasing of the coronagraph and removing differential tip/tilt between the interferometer arms. The mirror has the same coating as the DM to minimize amplitude and phase differences in the two arms of the interferometer. This nuller will be supplied with phase plates that will produce the pseudo-achromatic π phase change. This nulling architecture is highly symmetric, and has been designed to deliver nulls of greater than 500K:1 over a 150 nm bandpass centered at 675 nm.

The nulling interferometer and calibration system interferometer share a common beam splitter: the re-combination beam splitter of the nuller is the split beam splitter for the calibration system. The bright (asymmetric) port of the nuller passes through a spatial filter that removes any wave front errors in the system up to the pinhole. It is then re-collimated to form the reference arm of the calibration interferometer. A subsequent calibration phasing mirror allows this reference wave front to be phase shifted. The other arm of the calibration interferometer is created from a beam that is removed from the science by a spectrally-neutral beam splitter. This light also passes through an identical pair of OAP's. This is a simple way of both matching the polarization properties and path length of the beam that is in the reference arm.

Both beams are recombined at the calibration recombination beam splitter. After a pair of fold mirrors and a merge prism, pupils that are conjugate to the DM get imaged onto the calibration camera. This camera is a powerful firewire CCD from Prosilica, Inc. It is easily integrated into our instrument-control software and has easily defined integration times, gains, regions-of-interest, etc. The front and back sides of the calibration beam splitter have a phase offset of $\pi/2$, so only two phase steps are required if the want to combine these images in four-bucket phase/visibility measuring algorithm.

The calibration beam splitter is well-matched to the nulling beam splitter (identical glass substrate, coating, wedge, and orientation) in order to minimize the effects of low contrast due to amplitude and dispersion mismatches. The system has only come together recently but has been phased for white light operation. A photograph of the calibration system is shown below in Figure 4.

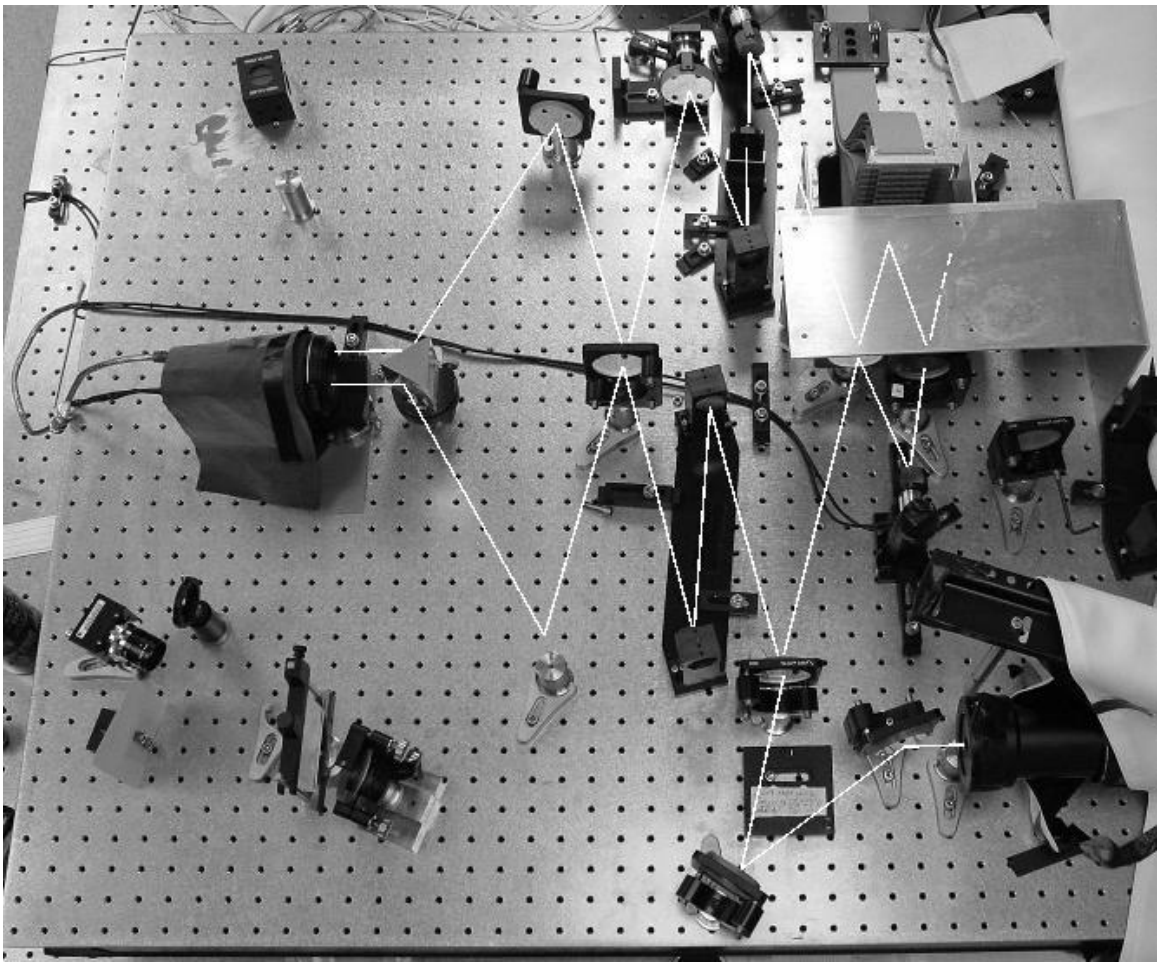

Fig. 4 Bird's-eye view of the calibration testbed. The souce/nulling coronagraph are on the right hand side of the image, while the calibration system is on center/left. The deformable mirror is covered by the sheet metel to protect if from contamination.

The science camera in our system is fed with a ~f/60 beam such that the core of the PSF from the calibration system can be sampled with ~ 10 pixels across it's full width. The camera is also tightly integrated into the control software. It has similar functionality as the calibration camera (selectable region of interest, integration time, etc.) but also has 16 bits of dynamic range and is cooled to minimize dark current.

2.2 Preliminary Results

The system, although only functional for a short time, has the ability to perform broad-band phase shifting interferometry on the nulling side of the system. A snap shot of this analysis is shown below. Once the deformable mirror and electronics are functioning well, the same operations for determining the complex wave front of the science wave front will be used with the calibration system. Indeed this will be done with the same software routines and same actuators to measure the amplitude and phase leakage terms. Thus, a highly functional nuller lends itself to rapid calibration system development.

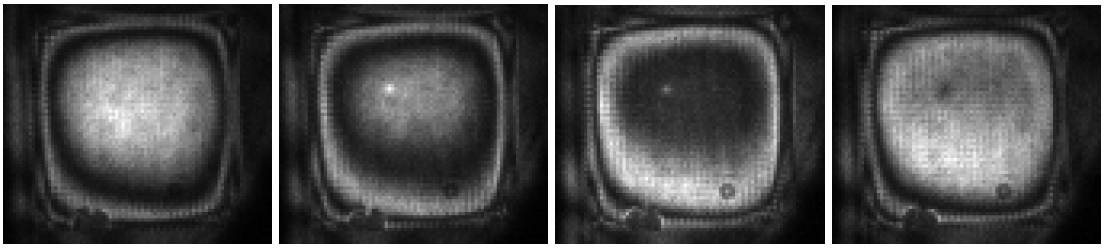

Fig. 5 Series of interferograms taken with the calibration testbed. These images are phase shifted by 90 degrees to derive the amplitude and phase of the complex wave front. The wave front defects (that appear as bright and dark spots) are due to local departures of DM pixels.

2.3 Future Plans: Gemini Planet Imager

As mentioned earlier, the goal of speckle calibration is critical for the future of direct detection of extra-solar planets. The work described here has been in support of the Gemini Planet Imager Instrument that is currently in the early planning stages. The coronagraph for this instrument will be an apodized pupil Lyot coronagraph: fundamentally, a much different coronagraph than the one used in the tesbed described above. However, we have designed a calibration system that is compatible with this instrument and its requirements. An image of our currently planned calibration system is shown in the image below.

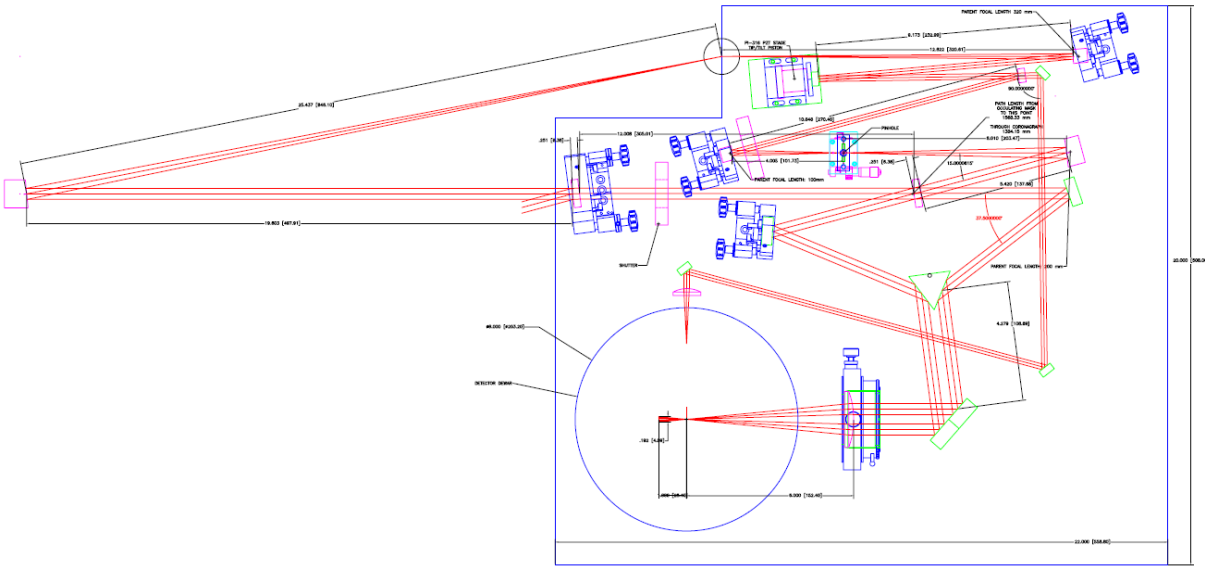

Fig. 6 Cartoon illustration of the opto-mechanical layout for the GPI calibration system. In this coronagraph, the science and reference arms are split in the image plane at the top center of the image.

In operation, this calibration system will take the light that passes through focal plane occulting spot to form the reference beam. This light is spatially filtered and re-collimated to interfere with a beam that is sampled from the science beam path. Both ports of the recombination beam splitter are imaged onto the infrared calibration detector. Although this system appears radically different than the calibration testbed, fundamentally they are identical.

During operation, the calibration wave front sensor will phase shift the reference wave front and then perform synchronous demodulation to extract the phase and amplitude components of the residual wave front. On slow time scales, ~ 0.5 to 1 minute, the system will feed phase errors to the adaptive optics system before the coronagraph. In this way, the residual speckles are continuously sensed and controlled.

The system does present some challenges related to the complexity of the instrument: it is a multi-national, multi-institution consortium with multitude of interactions and interfaces. Design of the system and the calibration unit will begin in earnest starting in June 2006. And after a few years of development, we may soon be able to make some of the first direct images of extra solar planets.

3. CONCLUSION

A method to suppress image plane speckles for planned and future planet-finding instruments has been described. A laboratory experiment to demonstrate this method is currently under development and showing early results. This calibration system is compatible with both imaging and nulling coronagraphs. Lessons learned from this work will be used in the development of the calibration system for the Gemini Planet Imager: GPI.

4. ACKNOWLEDGEMENTS

This work was carried out by the Jet Propulsion Laboratory, California Institute of Technology, under contract with the National Aeronautics and Space Administration. This work has been supported in part or full by the National Science Foundation Science and Technology Center for Adaptive Optics, managed by the University of California at Santa Cruz under cooperative agreement No. AST-9876783

REFERENCES

1. www.planetquest.jpl.nasa.gov/atlas/atlas_search.cfm
2. B. Macintosh, et. al., The Gemini Planet Imager, Proc SPIE, Astronomical Telescopes and Instrumentation, these proceedings.
3. J. Goodman, *Introdution to Fourier Optics, 2nd Ed.*, p.220, McGraw-Hill, 1996.
4. S. Shaklan, D. Moody, and J. Green. Residual Wave Front Phase Estimation in the Reimaged Lyot Plane for the Eclipse Coronagraphic Telescope. Proc. SPIE vol. 4860 (Waikaloa, 2002).
5. O. Guyon, "Imaging Faint Sources within a speckle halo with synchronous interferometric speckle subtraction", *ApJ*, 615, 562-572, 2004.
6. J. Codona & R. Angel, *ApJL*, 604, L125, 2004.
7. K. Creath, ''Phase-measurement interferometry techniques,'' in *Progress in Optics XXVI,* E. Wolf, ed. (Elsevier, New York, 1988), Chap. 5.
8. J. K. Wallace, et. al., Experimental results from the optical planet detector interferometer, Proc. SPIE vol. 5170, pp. 209-216 (San Diego 2003).